ChemElectroChem

Research Article
doi.org/10.1002/celc.202300677

Chemistry Europe
European Chemical Societies Publishing

www.chemelectrochem.org

Coupling of Phthalocyanines with Plasmonic Gold Nanoparticles by Click Chemistry for an Enhanced Singlet Oxygen Based Photoelectrochemical Sensing

Shahid U. Khan,[a, b, c] Refilwe Matshitse,[f] Rituraj Borah,[b, c] Manjunatha Nemakal,[f] Ekaterina O. Moiseeva,[d, e] Tatiana V. Dubinina,[e] Tebello Nyokong,[f] Sammy W. Verbruggen,[b, c] and Karolien De Wael*[a, c]

Coupling photosensitizers (PSs) with plasmonic nanoparticles increases the photocatalytic activity of PSs as the localized surface plasmon resonance (LSPR) of plasmonic nanoparticles leads to extreme concentration of light in their vicinity known as the near-field enhancement effect. To realize this in a colloidal phase, efficient conjugation of the PS molecules with the plasmonic nanoparticle surface is critical. In this work, we demonstrate the coupling of phthalocyanine (Pc) molecules with gold nanoparticles (AuNPs) in the colloidal phase via click chemistry. This conjugated Pc-AuNPs colloidal system is shown to enhance the photocatalytic singlet oxygen ($^1O_2$) production over non-conjugated Pcs and hence improve the photoelectrochemical detection of phenols. The plasmonic enhancement of the $^1O_2$ generation by Pcs was clearly elucidated by complementary experimental and computational classical electromagnetic models. The dependence of plasmonic enhancement on the spectral position of the excitation laser wavelength and the absorbance of the Pc molecules with respect to the wavelength specific near-field enhancement is clearly demonstrated. A high ~ 8 times enhancement is obtained with green laser (532 nm) at the LSPR due to the maximum near-field enhancement at the resonance wavelength.

Introduction

Photoelectrochemical (PEC) measurements, a newly developed analytical technique, have attracted considerable attention because of the combination of optics and electrochemistry. It possesses several advantages, such as fast response, high sensitivity, and low undesired background.[1–4] This technique shows highly promising analytical applications and has received extensive research interest in medicine,[5] environmental monitoring,[6] and (bio)sensing.[7–9] The efficiency of the PEC detection strongly depends on the properties of the photoactive materials, which play a crucial role in the enhancement of the response signal.[10,11] The photoactive materials in the PEC process are capable of harvesting light photons and create an electronic transition, which results in the formation of photogenerated carriers that supply the necessary energy for the redox reactions. In the last few years, photoactive materials including semiconducting oxide based materials,[2] semiconductor quantum dots,[12] and metal nanoparticles[13] have been exploited for PEC analysis. Generally, compared with these semiconductor based nanomaterials, molecular PSs possesses several advantages.

Molecular PSs such as Pcs have caused great interests and are widely exploited in the field of photocatalysis, PEC sensing and photosensitive solar cells due to their remarkable thermal and chemical stability, high extinction coefficient, excellent ability to harvest light and exceptional PEC performance.[14–16] In addition, the Pcs structural flexibility allows for modification and binding with the desired material through the functional groups.

Over the past years, researchers have revealed that coupling Pcs with other nanomaterials is an effective solution to improve the performance of such hybrid materials.[4,17] Nevertheless, the majority of previously reported PEC sensors employing Pcs have relied on the mechanism of photoinduced electron transfer from Pcs to a semiconductor, succeeded by electron transfer

[a] S. U. Khan, K. De Wael
A-Sense Lab, University of Antwerp, Groenenborgerlaan 171, 2020 Antwerp, Belgium
E-mail: karolien.dewael@uantwerpen.be

[b] S. U. Khan, R. Borah, S. W. Verbruggen
Sustainable Energy, Air & Water Technology (DuEL), Department of Bioscience Engineering, University of Antwerp, Groenenborgerlaan 171, 2020, Antwerp, Belgium

[c] S. U. Khan, R. Borah, S. W. Verbruggen, K. De Wael
NANOlab Center of Excellence, University of Antwerp, Groenenborgerlaan 171, 2020 Antwerp, Belgium

[d] E. O. Moiseeva
Skolkovo Institute of Science and Technology, 3 Nobelya Str., Moscow 121205, Russia

[e] E. O. Moiseeva, T. V. Dubinina
Department of Chemistry, Lomonosov Moscow State University, 119991 Moscow, Russian Federation

[f] R. Matshitse, M. Nemakal, T. Nyokong
Institute for Nanotechnology Innovation, Rhodes University, Makhanda, South Africa

Supporting information for this article is available on the WWW under https://doi.org/10.1002/celc.202300677

from the semiconductor to an electrode.[4] Our research group, however, has recently reported a novel PEC sensing approach that employs Pcs, resulting in the generation of $^1O_2$ upon illumination.[8,18,19]

However, in order to reach high sensitivities required for many applications, the molecular Pcs alone are not enough. Thus, the incorporation of components for optical enhancement in the photoactive nanomaterials to obtain hybrid nanostructures is necessary. In this regard, coupling Pcs with metal plasmonic nanoparticles such as AuNPs has received a wide attention because of their strong absorption and concentration of visible light through their surface plasmon resonance (SPR) property which results in the enhancement of $^1O_2$ generation by Pcs.[20–22] Wichmann *et al.* reported that the $^1O_2$ generation efficiency of Zinc Pc is enhanced by nearly an order of magnitude when it is linked with AuNPs.[21] Different shapes and sizes of AuNPs linked with Pcs following different strategies have been reported.[22] Such hybrid materials are typically used in photodynamic therapy (PDT), photooxidation reactions and to enhance the photophysical and non-linear optical properties of Pcs.[23–25] However, the control of the molecular Pcs and metal nanoparticles conjugation is still a challenging task due to the high precision and selectivity required to obtain well defined hybrid nanostructures.[22]

In this work, we successfully couple Pc with AuNPs for the PEC sensing of phenolic compound. Spherical citrate stabilized AuNPs were synthesized using the well-known Turkevich method.[26,27] The AuNPs were further functionalized with azidothiol linker. For the coupling of AuNPs with Pc, the click reaction was chosen due to the high yield of the product.[28] The schematic illustration of the coupling of AuNPs with ZnPc via click chemistry is shown in scheme 1. The ZnPc-AuNPs conjugate was characterized thoroughly using ultraviolet-visible (UV-Vis), Fourier-transform infrared spectroscopy (FTIR), transmission electron microscopy (TEM), and x-ray diffraction (XRD). The $^1O_2$-based PEC activity of the ZnPc-AuNPs conjugate was tested in an organic solvent (methanol) and the plasmonic enhancement of the $^1O_2$ generation by Pcs was demonstrated by a complementary experimental and theoretical investigation. The $^1O_2$ quantum yield of ZnPc alone and ZnPc clicked with AuNPs was measured using an indirect method, and a significant increase in the photocatalytic $^1O_2$ production was observed for ZnPc-AuNPs due to a synergistic effect between the plasmon resonance of AuNPs and ZnPc which subsequently enhances the PEC activity towards the sensing of hydroquinone (HQ).

Experimental

Materials and Methods

Materials. Bromo *tris*(triphenylphosphine) copper(I) ($Cu(PPh_3)_3Br$), triethylamine (Et_3N), gold (III) chloride trihydrate ($HAuCl_4{\times}3H_2O$), unsubstituted phthalocyaninato zinc (II), 1,3-diphenylisobenzofuran (DPBF), tetrabutylammonium fluoride (TBAF) 1.0 M in tetrahydrofuran (THF), and sodium citrate were purchased from Sigma Aldrich. Hydroquinone (HQ, 99.5%) and lithium chloride anhydrous (LiCl, 99%) were purchased from Acros, Belgium. Methanol (MeOH, 99.8% HPLC grade) and acetic acid (CH_3COOH, analytical reagent grade) were purchased from Fisher Chemical. Dimethylformamide (DMF), dimethyl sulfoxide (DMSO) were purchased from Merck. SH-$(CH_2)_{11}$-N_3 (11-azido-1-undecanethiol or azidothiol) (>95% purity) was purchased from Prochimica surfaces, Poland.

Characterization. For the UV-Vis spectroscopy of AuNPs and Pcs, a Shimadzu UV 2550 spectrophotometer was used. Attenuated transmittance reflection-Fourier transform infrared (ATR-FTIR) spectra were collected in the range of 4000 and 400 cm^{-1} using a Bruker Alpha II machine with a DTGS detector. For each sample, 128 scans were accumulated with a resolution of 4 cm^{-1}.

The morphology of AuNPs was characterized by using a JEOL TEM 1210 transmission electron microscope at 120 kV accelerating voltage. The samples were prepared by drop casting small amounts of the nanoparticle colloid on copper grids. X-ray powder diffraction patterns were recorded on a Bruker D8 Discover equipped with a LynxEye detector, using CuKα radiation (λ = 1.5405 Å, nickel filter). The zeta potential was measured by using a Malvern Zetasizer Nanoseries, Nano-ZS90.

Electrochemical measurements were carried out using an Autolab Potentiostat PGSTAT 302 N from Metrohm (Utrecht, The Netherlands). A double junction Ag/AgCl (1 M LiCl, Metrohm) electrode and a platinum wire were used as the reference and the counter electrodes respectively. Graphite rods (spectroscopically pure graphite, 3 mm in diameter, SPI Supplies Inc.) insulated from side walls with epoxy resin were used as working electrode. The diode lasers of wavelength 659 nm, and 532 nm (Roithner Lasertechnik,

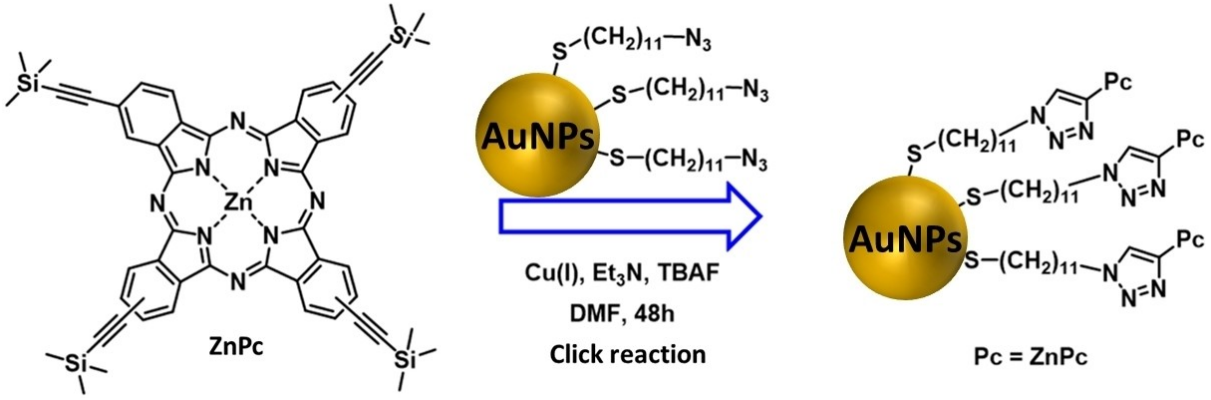

Scheme 1. Schematic representation of coupling of ZnPc to AuNPs via click chemistry approach in the presence of Cu(I) catalyst.

Austria) were used to illuminate the working electrode with an intensity of 30 mW (pre-adjusted using a light power meter). The illuminated area was 0.07 cm^2 (a circle of 3 mm in diameter) and corresponded to the area of the working electrode.

Triplet state quantum yields were determined using a laser flash photolysis system consisting of an LP980 spectrometer with a PMT-LP detector and an ICCD camera (Andor DH320T-25F03). The signal from a PMT detector was recorded on a Tektronix TDS3012 C digital storage oscilloscope. The excitation pulses were produced by a tunable laser system consisting of a Nd:YAG laser (355 nm, 135 mJ/4–6 ns), pumping an optical parametric oscillator (OPO, 30 mJ/3–5 ns) with a 420 to 2300 nm (NT-342B, Ekspla) wavelength range. Samples were prepared in deoxygenated DMSO by bubbling with argon for 20 min.

Synthesis of photosensitizer. 2(3),9(10),16(17),23(24)-tetra-(2-trimethylsilylethynyl) phthalocyaninato zinc (II) (ZnPc) (Scheme S1) was prepared using approach described earlier.[29] Briefly, 2(3),9(10),16(17),23(24)-Tetraiodophthalocyaninato zinc (II) (190 mg, 0.18 mmol), $Pd(PPh_3)_2Cl_2$ (10 mg, 0.01 mmol, 2 mol%), CuI (3 mg, 0.02 mmol, 4 mol%), and PPh_3 (8 mg, 0.03 mmol, 4 mol%) were placed in an argon-filled Schlenk flask. After the addition of 2 mL of freshly distilled triethylamine and 4 mL of dry THF the mixture was stirred at room temperature for 15 min and (trimethylsilyl)acetylene (40 mg, 0.87 mmol) was added. After that the mixture was stirred under argon at room temperature for 18 h and then evaporated under reduced pressure. The MeOH-H_2O (volume ratio 10:1) was added to precipitate the product, which was then filtered and washed with water and MeOH, to give 160 mg (94%) of the complex ZnPc. The synthetic pathway of ZnPc is shown in scheme S1.

Synthesis of AuNPs. 0.1470 g (5 mM) of sodium citrate was added into two neck round bottom flasks containing 99 mL of water and brought it to boil. Under vigorous stirring 1 mL of 25 mM gold precursor (gold (III) chloride trihydrate) was added and the reaction mixture was left at the boiling temperature for 15 mins. The obtained wine-red color of the solution indicated the formation of AuNPs.

Functionalization of AuNPs with 11-azido-1-undecanethiol and coupling to ZnPc via click reaction. The synthesized AuNPs were modified with 11-azido-1-undecanethiol as previously described.[30] Briefly, 18 μl of 11-azido-1-undecanethiol (4.21 M) was added to 100 mL of citrate stabilized AuNPs solution in water with sonication. The color of the solution changed from red to violet indicating the modification of AuNPs with azidothiol. The violet solution was centrifuged for 10 min at 10000 rpm and the resulting precipitate was redissolved in DMF. Following modification, click reaction was performed by adding 10 mg of ZnPc (1.04×10^{-2} mol) ($Cu(PPh_3)_3Br$) (50 mg, 0.054 mmol), 100 μL of azidothiol-AuNPs, 0.5 mL DMF, and 0.5 mL triethylamine. TBAF (1 M, 0.66 mL) was added dropwise (the first portion of 0.11 mL over 1 h and the second portion of 0.55 mL over 1.5 h), and the reaction mixture was stirred for 72 h under nitrogen atmosphere. The product was washed with MeOH three times and dried at room temperature for characterization.

Photophysical parameters. The $^1O_2$ and fluorescence quantum yield in DMSO for ZnPc, and ZnPc clicked to AuNPs were calculated using comparative methods reported elsewhere.[25] Singlet oxygen quantum yield (Φ_Δ) values are determined under ambient conditions using DPBF as a specific $^1O_2$ probe in DMSO. Unsubstituted ZnPc in DMSO was used as a standard $\Phi_\Delta = 0.67$ in DMSO.[31] The absorbance of DPBF should be twice as much as the absorbance of Pcs (2:1) DPBF:Pc ratio. Equal-volume of quencher and photocatalyst was measured to conduct the $^1O_2$ study. To measure, 1 ml of DPBF and 1 ml of Pcs were mixed together in the cuvette and illuminated it with 670 nm laser at different time intervals. The absorbances of DPBF are spectroscopically monitored at 417 nm at predetermined time intervals. For fluorescence quantum yield (using unsubstituted phthalocyaninato zinc (II), as a standard, with $\Phi_F = 0.20$[31] all samples were excited at 670 nm and their emission spectra recorded from 600 nm to 800 nm. The solution of ZnPc, and ZnPc clicked to AuNPs for triplet state studies were flushed with argon for 20 min before measurements. Next, the lifetime was calculated by fitting the experimental datasets to single exponential using OriginPro 2015 program.

Photoelectrochemical measurements. All electrochemical measurements were conducted in a three-electrode configuration with an upward-facing working electrode as described previously unless mentioned otherwise.[18] The working electrolyte solution was prepared by mixing 3.675 mL CH_3OH, 0.500 ml LiCl (0.1 M), 25 μL CH_3COOH (AcOH) (5 mM), 250 μL CH_3COONa (AcONa) (5 mM), 500 μL PS (50 μM) and 50 μL of HQ (1 mM) which makes a total volume of 5 mL. The stock solutions of all the above components were prepared in CH_3OH. For the blank measurements, i.e. in the absence of HQ or the photosensitizer, the total volume of 5 mL was maintained by the addition of CH_3OH. The beam of the diode laser was directed to the working electrode to measure the photocurrents. Prior to use, the working electrodes were polished on wet grinding paper (GRIT 800, Buehler) for 1 min, then sonicated for 20 sec in deionized water and dried in air.

Results and Discussion

Characterization of AuNPs and AuNPs-ZnPc conjugated systems. For plasmonic enhancement with AuNPs, the NPs need to be large enough (>10 nm) so that the plasmonic response from the free electron cloud is sufficiently strong and the quantum size effects are not significant.[32] The ~14.1 ± 1.3 nm NPs as obtained by the synthesis procedure are thus suitable for the present work. As shown in Figure 1 (a) and (b), the TEM imaging of the NPs confirms the spherical shape and relatively monodisperse size distribution. It is known that the extent of plasmonic near-field enhancement increases with nanoparticle size up to ~50 nm and decreases thereafter.[33]

It is important to note that with increasing size, the surface area per unit of mass of the NPs also decreases.[34] Thus, for the present work, the ~ 15 nm NPs are small enough to ensure large surface area while still exhibiting a strong plasmonic response. To combine these NPs with the photosensitizer via click chemistry, a linker molecule is required that can strongly bond with the AuNPs. The azidothiol molecules form the strong -S-Au- bond and an azide group remains at the free end.[22,30] The click chemistry catalyzed by the Cu(I) can thus facilitate the bonding between the Pc and the azide group to form a strong AuNPs–Pc linkage as shown in Scheme 1. The successful modification of AuNPs with azidothiol was further confirmed by measuring the zeta potential. Figure 1 (c) shows the Zeta potential of as-prepared citrate-stabilized AuNPs was found to be −30.1 mV. After modification with azidothiol the zeta potential value changed to +15.1 mV. This value confirms that AuNPs are capped by the azidothiol linker.[35]

UV-Vis spectroscopy was used to characterize the strong optical properties of both the AuNPs and the Pcs. Firstly, when the AuNPs are functionalized with the linker molecules

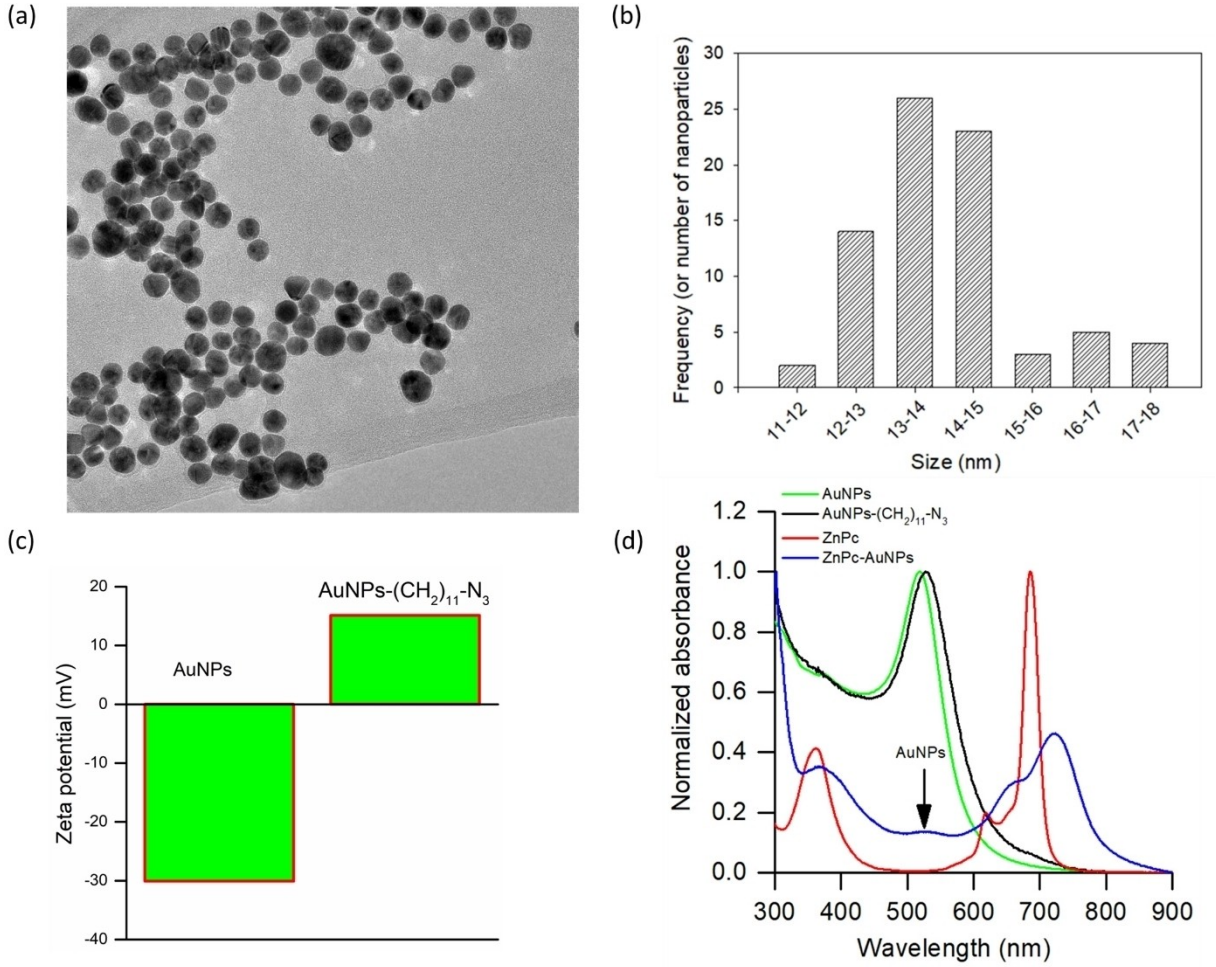

Figure 1. (a) Transmission electron microscope (TEM) images of bare AuNPs. (b) AuNPs size distribution obtained from TEM imaging. The average size from 78 data points is 14.1 nm with a standard deviation of 1.3 nm. (c) Zeta potentials of AuNPs and Azidothiol capped AuNPs. (d) UV-vis spectra of unmodified AuNPs, AuNPs modified with linker (AuNPs-$(CH_2)_{11}$-N_3), ZnPc and ZnPc-AuNPs in DMF.

(azidothiol), no significant change in the spectra was observed as the only changes could be a slight (up to ~10 nm) red shift of the plasmon band at 530 nm due to the change in the dielectric environment around the NPs (*i.e.* the azidothiol shell and DMF solvent), Figure 1 (d). The blue curve in Figure 1 (d) suggests the conjugation of the Pc with AuNPs. Interestingly, since the Pc and the AuNPs are now in close proximity, a linear relationship between the concentration of the two entities and the intensity according to the Beer-Lambert law does not hold. Thus, the mutual interaction between the Pc and AuNPs results in the optical spectra of the AuNPs–Pc 'clicked' samples. It is expected here that the near-field enhancement of AuNPs concentrate light in their vicinity to provide the Pcs a higher exposure than the usual isolated molecules. Thus, a stronger absorption per molecule takes place in this case as compared to Pc molecules in absence of AuNPs. In the UV-Vis spectrum, a relatively stronger intensity is observed for the Pcs while the Au plasmon band is weakened. Also, a shift of the Q band of the Pc from 685 nm to 721 nm after conjugation with AuNPs indicates the close proximity of the Pc molecules and the AuNPs that leads to changes in the energy levels. Similarly, the shoulder at ~533 nm in the optical spectra of the Pc signifies such nanoparticle-Pc interaction.

FTIR characterization of Pc-AuNPs conjugates. Figure 2 (a) shows the FTIR spectrum of azidothiol and azidothiol capped AuNPs. The sharp intense band at 2090 cm^{-1} is characteristic for the azide stretching vibration (N_3). The presence of azidothiol capped on the surface of AuNPs was confirmed by a small N_3 band at 2096 cm^{-1}. The minor shift and reduction in intensity of the N_3 band after capping on AuNPs confirmed interaction between the azidothiol and AuNPs. The CH/CH_2 stretching vibrations at 2870 cm^{-1} and 2955 cm^{-1} can also be seen after the capping of AuNPs. Figure 2 (b) shows the FTIR spectrum of ZnPc, and ZnPc after click reaction. The characteristic band at 2143 cm^{-1} is assigned to the stretching vibration of C≡C and bands at 2850–2940 cm^{-1} are assigned to the stretching vibration of C–H. Importantly, the band at 2143 cm^{-1} assigned to C≡C disappeared after click reaction with azidothiol capped AuNPs. The disappearance of C≡C, and appearance of a new band again confirms the successful click reaction and therefore coupling of AuNPs to Pc.

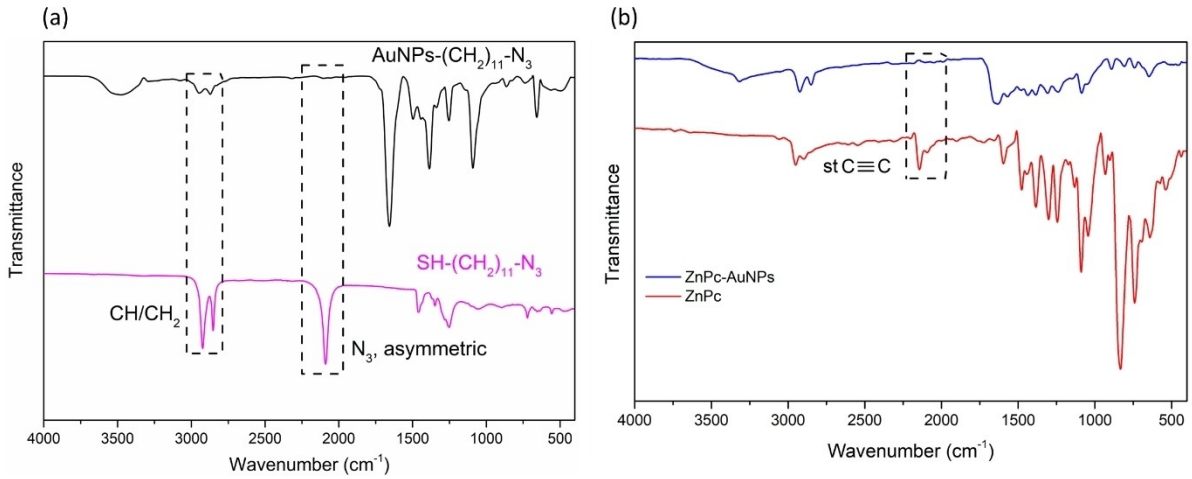

Figure 2. (a) FTIR spectra of azidothiol (pink) and azidothiol capped AuNPs (black). (b) FTIR spectra of ZnPc (red) and ZnPc-AuNPs after click reaction (blue).

XRD characterization of ZnPc-AuNPs conjugates. The X-ray diffraction patterns of as-synthesized citrate-stabilized AuNPs, ZnPc, and ZnPc conjugated with AuNPs are shown in Figure 3. The AuNPs in Figure 3 (a) showed five well-defined diffraction peaks with experimental 2θ values at 38.1° (111), 44.2° (200), 64.5° (220), 77.8° (311), and 81.8° (222). All the observed peaks correspond to standard Bragg's reflections and are consistent with the reported data.[36] Due to the amorphous nature of the Pcs, broad peaks in the range of 17°–26° are observed in Figure 3 (b) with typical lattice indices (400) and (600).[37] Previous studies have indicated that the presence of metalated Pc composites gives rise to distinctive XRD peaks within the 2θ range of 21° to 30°. These peaks can be attributed to the electron density originating from Pc, leading to modifications in the tilt angle and alterations in the intensity distribution observed in the XRD diffraction pattern.[37] The diffraction peak of AuNPs can be seen in Figure 3 (c) after click reaction with ZnPc as a very broad noisy peak at 17°–26°.

Triplet lifetime of ZnPc and ZnPc-AuNPs. The triplet lifetimes of ZnPc and ZnPc-AuNPs conjugate were determined using laser flash photolysis. Figure 4 shows the triplet decay curves of ZnPc and ZnPc clicked to AuNPs and the triplet lifetimes are shown in Table 1. The observed triplet lifetime of ZnPc-AuNPs conjugates (69.9 μs) was higher than that of the ZnPc alone (49.3 μs), Table 1. The increase in the lifetime suggests that the ZnPc is protected by AuNPs as the size of AuNPs is much larger than the Pc ~ 1 nm.[38,39] This increase in the triplet lifetime is consistent as reported by Mthethwa *et al.* with ZnPcSH and ZnPcSH-AuNP.[40]

Table 1. Photophysicochemical properties of AuNPs, AuNPs–S-$(CH_2)_{11}$-N_3, ZnPc and ZnPc-AuNPs in DMSO.

Sample	λ_{abs} (nm)	z (mV)	τ_T(μs)	Φ_Δ
AuNPs	522	−30.1	–	0.037[45,46]
AuNPs–S-$(CH_2)_{11}$-N_3	530	+15.1	–	–
ZnPc	685	–	49.3	0.56
ZnPc-AuNPs	721	–	69.9	0.66

λ_{abs} = absorption wavelength; z = zeta potential; τ_T = triplet lifetime.

Singlet oxygen quantum yield. $^1O_2$ generation depends on the energy transfer from the triplet state of the photosensitizer to ground state molecular oxygen. Thus, the $^1O_2$ quantum yield is a measure of the efficiency of the processes involving in the generation of $^1O_2$. Therefore, in order to determine the $^1O_2$ quantum yield of ZnPc and ZnPc-AuNPs, the chemical photodegradation of a $^1O_2$ probe, DPBF, in DMSO was monitored over a period of time (Figure 5) under ambient conditions. The absorption band of DPBF at 417 nm gradually decreased with increasing irradiation time while the Q band of Pc did not change, indicating the Pcs photostability. A significant increase in $^1O_2$ generation was observed as proven by the $^1O_2$ quantum yield (Table 1) after conjugation of ZnPc with AuNPs. The following equation as described in the literature[41,42] was used to determine the $^1O_2$ quantum yield:

$$\Phi_{\Delta} = \Phi_{\Delta(std)} \times \frac{R.\ I^{Std}{}_{abs}}{R^{Std}.I_{abs}}$$

where Φ_Δ is the singlet oxygen quantum yields for the standard ZnPc. R and R_{Std} are the DPBF photobleaching rates in the presence of the respective samples and standard, respectively. I_{abs} and I_{Std} abs are the rates of light absorption by the samples and standard, respectively. The $^1O_2$ quantum yields of ZnPc, and ZnPc-AuNPs were found to be 0.56 and 0.66, respectively, Table 1, and these values are consistent with the findings reported in the existing literature for similar systems.[43,44] The increase in the Φ_Δ value for ZnPc-AuNPs can be attributed to the plasmon resonance of AuNPs. Moreover, the $^1O_2$ of AuNPs alone is very low as reported previously,[45,46] meaning that the AuNPs can generate $^1O_2$ when conjugated with PSs such as Pcs. The heavy atoms of AuNPs encourage intersystem crossing to the triplet state of the Pcs, enhancing the Pcs triplet population and thus $^1O_2$ quantum yield.

Photoelectrochemical hydroquinone detection with ZnPc-AuNP conjugates. The $^1O_2$-based PEC activity of ZnPc and ZnPc-AuNPs was measured in MeOH to investigate the plasmon enhancement in the ZnPc-AuNPs conjugated system. The PEC detection mechanism is based on $^1O_2$ produced by illuminating the solution with a

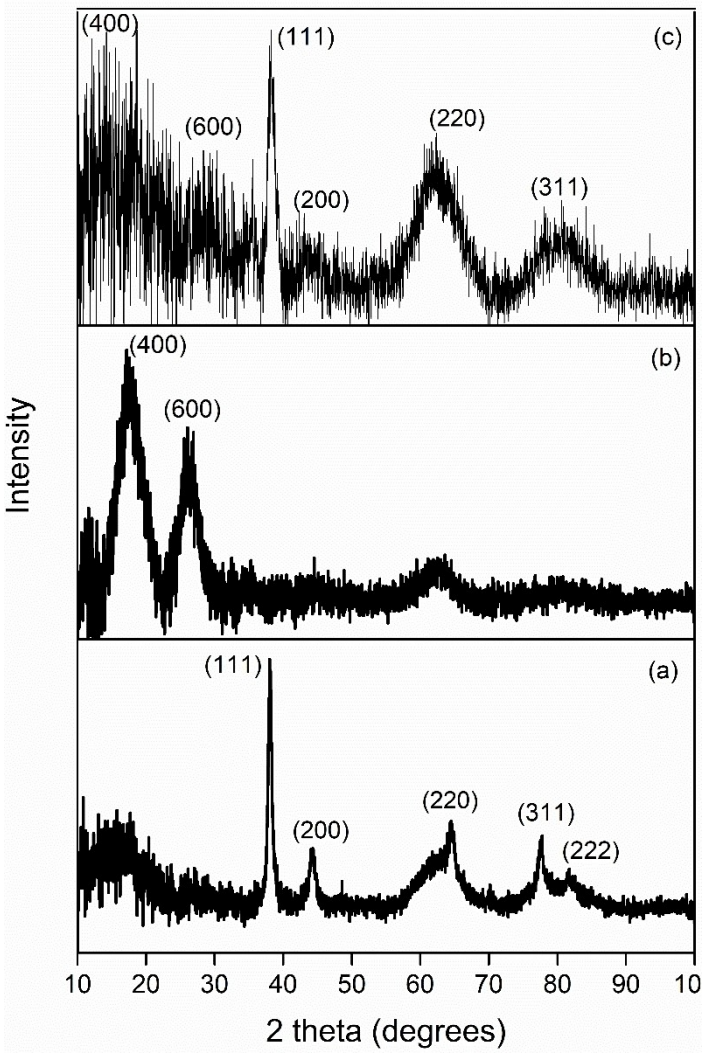

Figure 3. X-ray diffraction pattern of citrate stabilized (a) AuNPs, (b) ZnPc, and (c) ZnPc-AuNPs after click reaction.

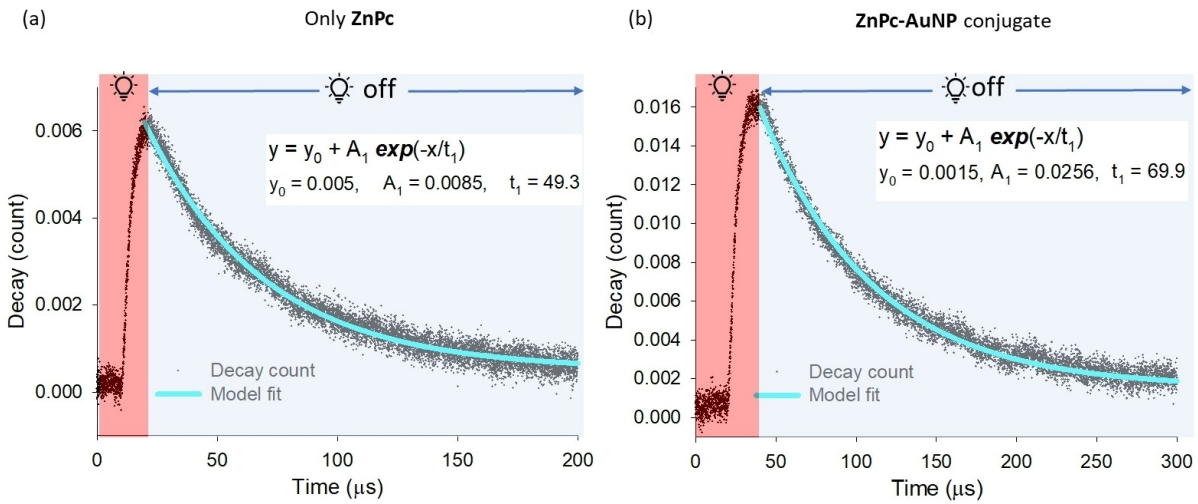

Figure 4. Triplet absorption decay curves for (a) ZnPc and (b) ZnPc-AuNP conjugates. The fitting to the exponential decay equation yields the triplet lifetime t_1. The goodness of fit is as follows: Figure (a): $R^2 = 0.9815$, Adj $R^2 = 0.9815$, Figure (b): $R^2 = 0.9852$, Adj $R^2 = 0.9852$.

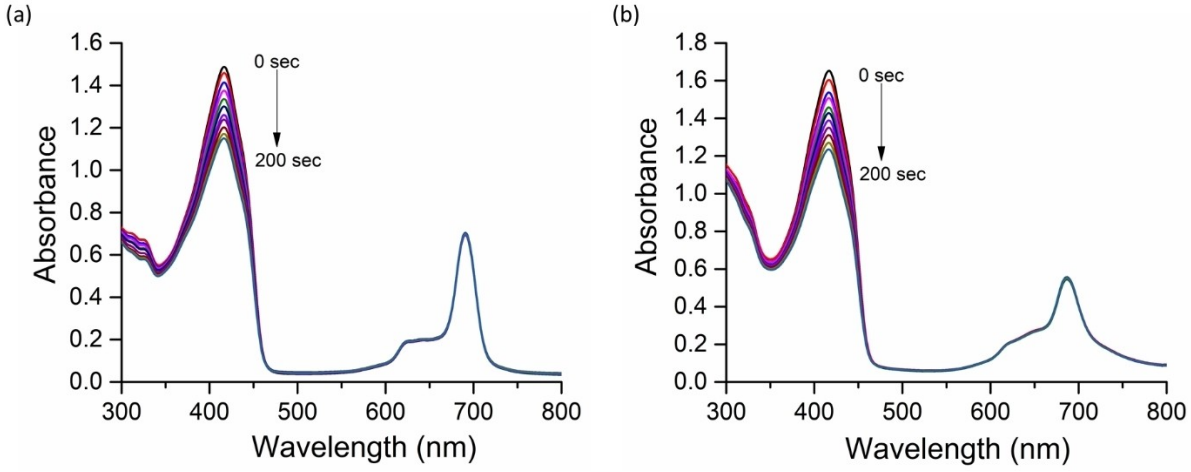

Figure 5. UV-Vis spectra for $^1O_2$ quantum yield determination using a photochemical method. Degradation of DPBF in the presence of (a) ZnPc and (b) ZnPc-AuNPs. The laser with wavelength 670 nm was used to illuminate the samples.

LED matching the wavelength of the absorbance maxima of the ZnPc, *i.e.* a peak emission wavelength at 659 nm. The produced $^1O_2$ oxidizes HQ which results in the formation of benzoquinone (BQ). By applying a negative potential of −0.1 V at a graphite working electrode BQ can be reduced back to HQ. The electrochemically reduced product, HQ, can react again with $^1O_2$, thus, initiating a catalytic redox cycle. This redox cycle amplifies the amperometric response of the phenols, measured as a quantifiable photocurrent (Figure 6 (a,d)). Thus, the larger $^1O_2$ production by the photosensitizer results in larger BQ production that also results in a stronger PEC response.

Photoelectrochemical measurements under red laser illumination. Figure 6 (a) depicts a typical amperometric response of the ZnPc and ZnPc-AuNPs in 1 mM HQ. Switching on the laser enables the immediate and accurate measurement of the photocurrent, and the background can be easily subtracted by simply switching off the laser. A photocurrent response of 250 nA was obtained when ZnPc was illuminated with 659 nm laser light as shown in Figure S1 (a). Clearly, the laser wavelength of 659 nm overlaps with the visible absorbance band (Q band) of ZnPc and hence, yields a fairly strong photocurrent response even without the AuNPs, Figure 6 (b). Now, the conjugation of AuNPs brings about a light concentration effect in the immediate vicinity where the ZnPc molecules are located, thereby further increasing $^1O_2$ production rate and hence the photocurrent response. This light concentration effect also known as the near-field enhancement is the intensification of the evanescent field around the NPs with respect to the incident electromagnetic field due to plasmonic excitation. The dotted line in Figure 6(b) shows that a maximum of a four-fold near-field enhancement can be obtained for 15 nm AuNPs upon excitation by 659 nm laser light, which is still >100 nm off from the LSPR position of the NPs at ~535 nm. The two dimensional (2D) near-electric field map in Figure 6 (c) shows that in theory, upon excitation at 659 nm a very local maximal field enhancement of a factor of four can be attained along the direction of the exciting field. Overall, an effective total enhancement of a factor of 3.4 in the photocurrent was observed in practice after the click reaction of ZnPc with AuNPs, Figure S1 (a), matching well with the theoretical prediction. While the 15 nm AuNPs have their plasmon band maximum at around 535 nm, still, upon excitation at 659 nm a field enhancement of a factor of >3 can still easily be attained over a significant volume around the NPs (Figure 6 (c)). Thus, with stronger optical absorption by Pcs in this region, a higher $^1O_2$ yield from the Pcs results in strong photocurrents by the HQ-BQ redox cycle. It shows that although the Q band of the Pc does not match perfectly with the LSPR of the NPs, the NPs can still provide a strong plasmonic enhancement with laser illumination matching the Q band.

Photoelectrochemical measurements under green laser illumination. As opposed to a red laser (659 nm), a green laser with a wavelength of 532 nm is significantly far from the Q band of ZnPc. Thus, the illumination of the bare ZnPc with a 532 nm laser naturally yields significantly lower $^1O_2$ and, hence, a lower photocurrent response of only 50 nA in contrast to ~250 nA with the 659 nm red laser, Figure 6 (d). However, as shown in Figure 6 (e), the 532 laser matches perfectly with the absorption maximum of the LSPR band of the AuNPs. This implies that the enhancement factor brought about by the AuNPs will be highest at this wavelength. As a result, after the conjugation of the AuNPs, the photocurrent is increased by more than eight times. As shown in Figures 6 (e) and (f), the theoretical near-field enhancement is more than 6-fold close to the particle surface, which is 50% higher compared to excitation by the red laser. Due to this significantly higher near-field enhancement at LSPR with green laser as compared to red-laser, a proportionately higher photocurrent increase (by a factor of eight) was also measured as shown in Figure S1 (b). In addition, the PEC activity of AuNPs alone was also tested in the presence of HQ (Figure S2) but no photocurrent response was observed, giving further evidence that AuNPs did not produce enough $^1O_2$ to oxidize the HQ molecule.

Effect of $^1O_2$ quencher. To confirm that the observed PEC response in both ZnPc, and ZnPc-AuNPs is in fact due to the $^1O_2$ generation, NaN_3, a well-known $^1O_2$ quencher was added and the photocurrent was measured. As shown in Figure 7, NaN_3 significantly suppressed the PEC activity by 27% for ZnPc and 30% for ZnPc-AuNPs at 1 mM NaN_3. Upon further increasing the concentration of NaN_3 to 10 mM the PEC activity is suppressed by 70% and 46% for ZnPc and ZnPc-AuNPs, respectively. However, the PEC activity for ZnPc-AuNPs is suppressed less and this could be due to aggregation of ZnPc after coupling with AuNPs as shown in UV-Vis spectra (Figure 1 (d), and when there is excess amount of NaN_3 these aggregates become shielded and thus less quenching sites become available. These experimental results are in accordance with our previous work,[18,19] and ascertain that $^1O_2$ is the predominant reactive oxygen species that are produced by both ZnPc and ZnPc-AuNPs upon illumina-

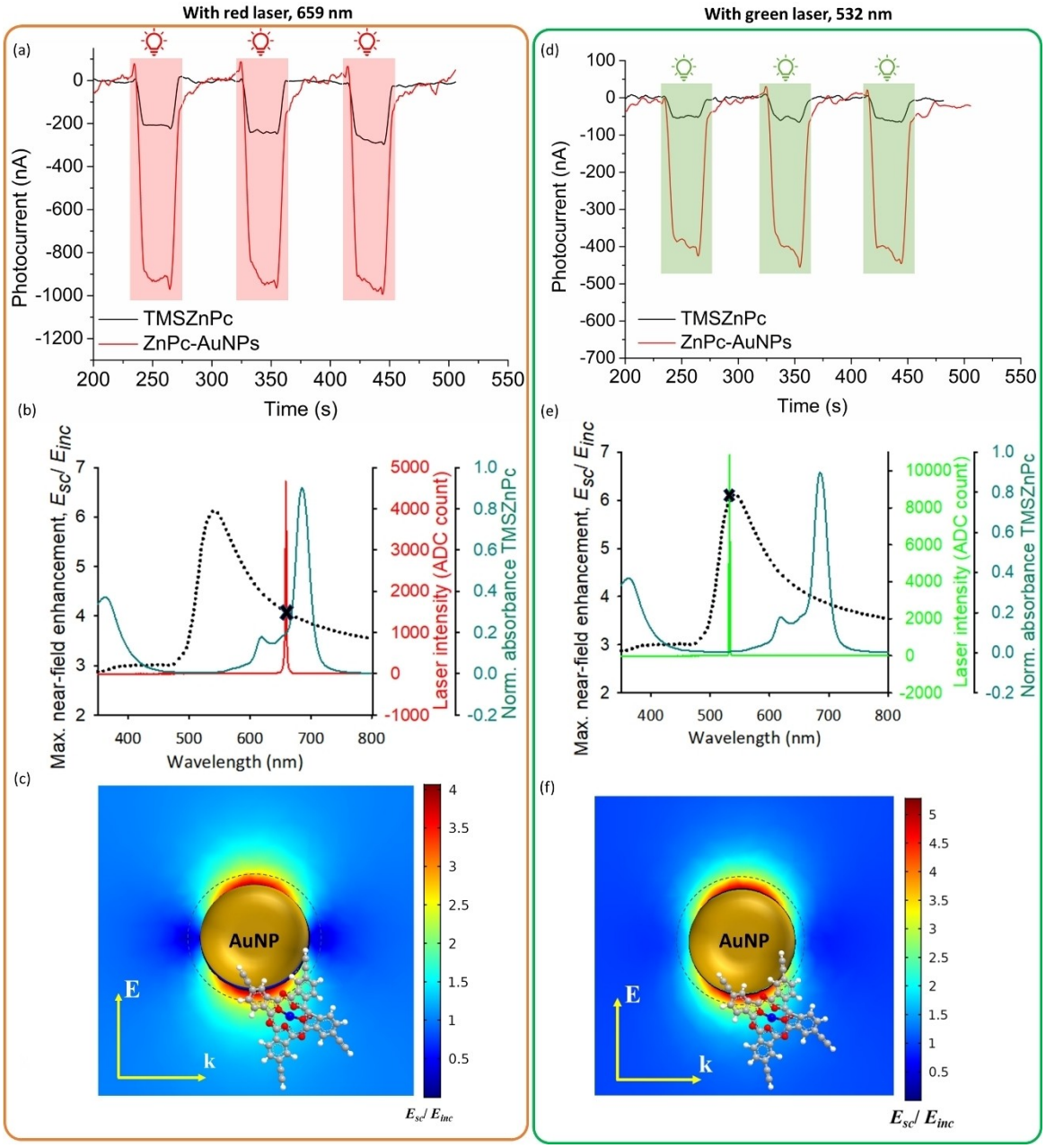

Figure 6. With red laser: (a) Amperometric behavior of ZnPc and ZnPc-AuNPs (in MeOH) in the presence of 1 mM HQ and the potential applied is −0.1 V. The measuring solution was illuminated with a red laser (659 nm, 30 mW). (b) discrete action spectrum: UV-Vis spectrum (cyan) of ZnPc overlaid with the near-field enhancement (dotted line) of the AuNPs and red laser intensity (red). (c) near-field enhancement with respect to incident wavelength of 659 nm around AuNPs. With green laser: (d) Amperometric behavior of ZnPc and ZnPc-AuNPs (in MeOH) in the presence of 1 mM HQ and the potential applied is −0.1 V. The measuring solution was illuminated with a green laser (532 nm, 30 mW). (e) discrete action spectrum: UV-Vis spectrum (cyan) of ZnPc overlaid with the near-field enhancement (dotted line) of the AuNPs and green laser intensity (green). (f) near-field enhancement with respect to incident wavelength of 532 nm around AuNPs.

tion, however, less effective in case of conjugated system which involves electron transfer mechanism.

Limit of detection and sensitivity. The limit of detection (LOD) for HQ with ZnPc alone, and ZnPc-AuNPs was determined under similar conditions with an applied potential of −0.1 V and under red laser (659 nm) illumination. The LOD value for HQ was calculated by dividing the standard deviations of blanks by the slope of the calibration curves. The calibration curve with ZnPc and ZnPc-AuNPs was established as shown in Figure 8(a) and 9(b). The LOD value for HQ with ZnPc was found to be 2.61 μM L^{-1} with a sensitivity of 0.00991 A M^{-1} cm^{-2}. The LOD for HQ with ZnPc-AuNPs was observed as the lowest LOD of 0.018 μM which is ~142 times lower than with ZnPc alone with a high sensitivity of 1.4883 A M^{-1} cm^{-2}.

Conclusions

In order to enhance the $^1O_2$ generation by Pc photosensitizers for sensing applications, Pc molecules were covalently linked

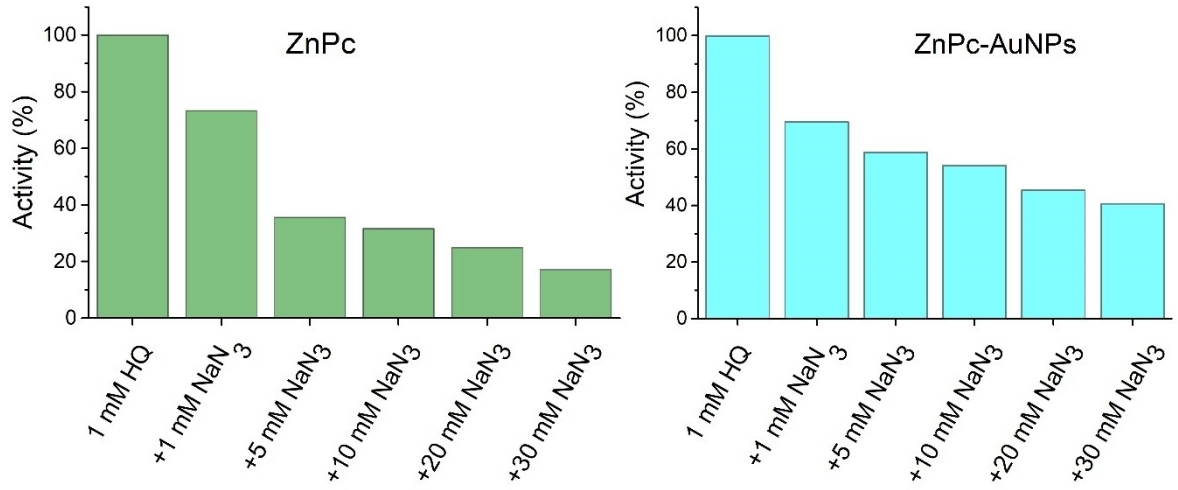

Figure 7. The effect of $^1O_2$ quencher NaN_3 on the photocurrent measured with ZnPc and ZnPc-AuNPs. The concentration of HQ and potential applied is kept constant as in earlier experiments, 1 mM, and −0.1 V, respectively. Red laser (659, 30 mW) was used to illuminate the measuring solutions.

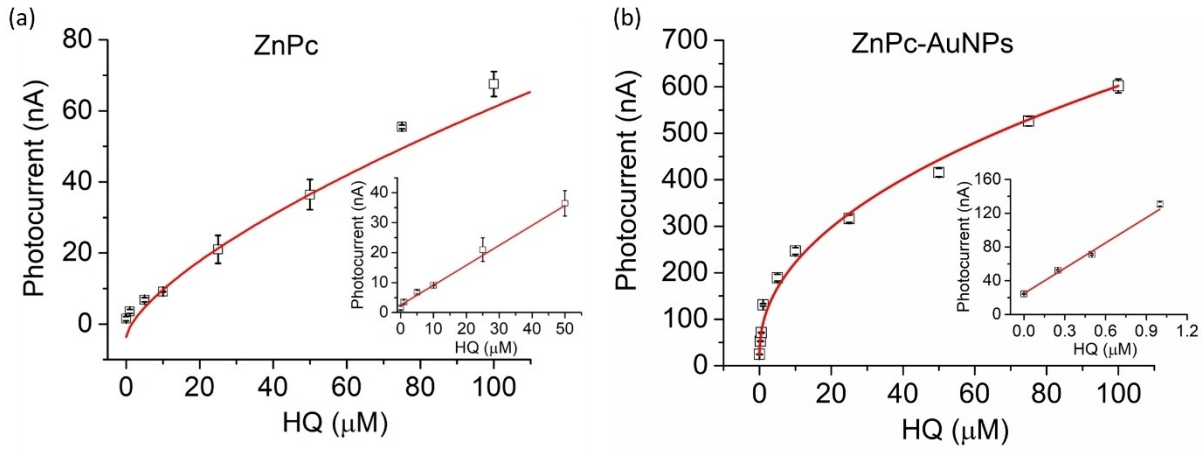

Figure 8. Calibration curve obtained for HQ at −0.1 V in the presence of (a) ZnPc (inset represents the linear curve in the concentration range of 50–1000 μM. (b) ZnPc-AuNPs (inset represents the linear curve in the concentration range of 1–100 μM. The measuring solution was illuminated with a red laser (659 nm, 30 mW). The error bars represents s.d. of three different electrodes.

with AuNPs by a click-chemistry procedure. The Au-thiol bond of the linker molecule ensures stable AuNPs-ZnPc conjugated units that are colloidally stable. The PEC quantification of the $^1O_2$ generation was measured based on a hydroquinone-benzoquinone redox cycle. The PEC quantification allows direct investigation of the photocurrent response with varying illumination conditions in real time. The photocurrent response of the ZnPc molecules is enhanced by AuNPs by their plasmonic effect. The effect of illumination at the LSPR and away from the LSPR clearly shows the variation in plasmonic enhancement. At the resonance (~532 nm), the plasmonic enhancement is significantly higher than the enhancement away from the resonance (~659 nm). On the other hand, even with a relatively lower plasmonic enhancement, the photocurrent at 659 nm is still much larger due to the illumination very close to the Q band of the Pc. This work shows the potential of AuNPs–Pc conjugated systems realized by click chemistry to be used in $^1O_2$-based applications such as PDT, antimicrobial activity and the detection of phenolic compounds. As AuNPs have already been investigated for photothermal therapy with success, conjugation of the Pcs as the PDT agent and Au nanoparticles as optical enhancement mechanism (apart from the photo-thermal effect) is a very promising hybrid material for such applications. Similarly, the antimicrobial activity of Pcs can be significantly improved by the incorporation of metal NPs. However, as the use of the AuNPs for large scale applications may be economically infeasible, other plasmonic metals such as Ag, Au or Cu can be promising candidates. Thus, the hybrid nanostructure demonstrated in this work also provides a general framework for the improvement of light driven applications of molecular Pcs.

Acknowledgements

The financial support by DOCPRO1 project funding from the University of Antwerp and a traveling grant to South Africa to Shahid U. Khan is gratefully acknowledged. FWO is acknowledged for funding. The work in South Africa was supported by the Department of Science and Innovation (DSI) and National Research Foundation (NRF), South Africa, through the DSI/NRF South African Research Chairs Initiative (UID 62620). We would also like to thank Prof. John Mack for his help in the triplet lifetime measurement.

Conflict of Interests

The authors declare no conflict of interest.

Data Availability Statement

The data that support the findings of this study are available from the corresponding author upon reasonable request.

[1] Y. Hu, Z. Xue, H. He, R. Ai, X. Liu, X. Lu, *Biosens. Bioelectron.* **2013**, *47*, 45.
[2] G. L. Wang, K. L. Liu, Y. M. Dong, X. M. Wu, Z. J. Li, C. Zhang, *Biosens. Bioelectron.* **2014**, *62*, 66.
[3] G. L. Wang, J. J. Xu, H. Y. Chen, S. Z. Fu, *Biosens. Bioelectron.* **2009**, *25* (4), 791.
[4] J. Shu, D. Tang, *Anal. Chem.* **2020**, *92* (1), 363.
[5] Z. Qiu, D. Tang, *J. Mater. Chem. B* **2020**, *8* (13), 2541.
[6] P. Yan, D. Jiang, H. Li, J. Bao, L. Xu, J. Qian, C. Chen, J. Xia, *Sens. Actuators B Chem.* **2019**, *279*, 466.
[7] C. Li, W. Lu, M. Zhu, B. Tang, *Anal. chem.* **2017**, *89* (20), 11098.
[8] S. Trashin, V. Rahemi, K. Ramji, L. Neven, S. M. Gorun, K. De Wael, *Nat. Commun.* **2017**, *8* (1), 16108.
[9] Q. Hao, P. Wang, X. Ma, M. Su, J. Lei, H. Ju, *Electrochem. Commun.* **2012**, *21*, 39.
[10] N. Haddour, J. Chauvin, C. Gondran, S. Cosnier, *J. Am. Chem. Soc.* **2006**, *128* (30), 9693.
[11] R. Gill, M. Zayats, I. Willner, *Angew. Chem. Int. Ed.* **2008**, *47* (40), 7602.
[12] R. Li, Y. Liu, T. Yan, Y. Li, W. Cao, Q. Wei, B. Du, *Biosens. Bioelectron.* **2015**, *66*, 596.
[13] S.A. Ansari, M. M. Khan, M. O. Ansari, M. H. Cho, *Sol. Energy Mater. Sol. Cells* **2015**, *141*, 162.
[14] C. G. Claessens, U. Hahn, T. Torres, *The Chem. Rec.* **2008**, *8* (2), 75.
[15] M. Urbani, M. E. Ragoussi, M. K. Nazeeruddin, T. Torres, *Coord. Chem. Rev.* **2019**, *381*, 1.
[16] D. Gounden, N. Nombona, W. E. van Zyl, *Coord. Chem. Rev.* **2020**, *420*, 213359.
[17] Q. Liu, T. Shi, Y. Cheng, Z. Wen, C. Ding, Y. Li, K. Wang, *J. Hazard. Mater.* **2021**, *406*, 124749.
[18] S. U. Khan, S. A. Trashin, Y. S. Korostei, T. V. Dubinina, L. G. Tomilova, S. W. Verbruggen, K. De Wael, *ChemPhotoChem* **2020**, *4* (4), 300.
[19] S. U. Khan, S. Trashin, V. Beltran, Y. S. Korostei, M. Pelmus, S. M. Gorun, T. V. Dubinina, S. W. Verbruggen, K. De Wael, *Anal. Chem.* **2022**, *94* (37), 12723.
[20] D. Steinebrunner, G. Schnurpfeil, J. Thayssen, J. A. T. Burgos, A. Wichmann, D. Wöhrle, A. Wittstock, *RSC adv.* **2021**, *11* (19), 11364.
[21] A. Wichmann, G. Schnurpfeil, J. Backenköhler, L. Kolke, V. A. Azov, D. Wöhrle, M. Bäumer, A. Wittstock, *Tetrahedron* **2014**, *70* (36), 6127.
[22] S. A. Majeed, K. E. Sekhosana, A. Tuhl, *Arab. J. Chem.* **2020**, *13* (12), 8848.
[23] O.M. Bankole, T. Nyokong, *J. Photochem. Photobiol., A* **2016**, *319–320*, 8.
[24] D. Steinebrunner, G. Schnurpfeil, M. Kohröde, A. Epp, K. Klangnog, J. A. T. Burgos, A. Wichmann, D. Wöhrle, A. Wittstock, *RSC Adv.* **2020**, *10* (39), 23203.
[25] E. Dube, D. O. Oluwole, N. Nwaji, T. Nyokong, *Spectrochim. Acta A Mol. Biomol. Spectrosc.* **2018**, *203*, 85.
[26] J. Turkevich, *Gold bulletin* **1985**, *18* (4), 125.
[27] J. Turkevich, P. C. Stevenson, J. Hillier, *Discuss. Faraday Soc.* **1951**, *11*, 55.
[28] M. Juríček, P. H. J. Kouwer, J. Rehák, J. Sly, A. E. Rowan, *J. Org. Chem.* **2009**, *74* (1), 21.
[29] E. O. Moiseeva, A. D. Kosov, N. E. Borisova, B. N. Tarasevich, T. V. Dubinina, L. G. Tomilova, *Inorganica Chim. Acta* **2022**, *535*, 120855.
[30] D. Baranov, E.N. Kadnikova, *J. Mater. Chem.* **2011**, *21* (17), 6152.
[31] M. Özdemir, G. Ö. Artuç, B. Akkurt, B. Yalçın, Ü. Salan, M. Durmuş, M. Bulut, *New J. Chem.* **2021**, *45* (22), 9912.
[32] R. Borah, S. W. Verbruggen, *Colloids Surf. A: Physicochem. Eng. Asp.* **2022**, *640*, 128521.
[33] C. Deeb, X. Zhou, J. Plain, G. P. Wiederrecht, R. Bachelot, M. Russell, P. K. Jain, *J. Phys. Chem. C* **2013**, *117* (20), 10669.
[34] M. Naito, T. Yokoyama, K. Hosokawa, K. Nogi, Third Ed.; Elsevier, **2018**.
[35] Z. Zhang, W. Li, Q. Zhao, M. Cheng, L. Xu, X. Fang, *Biosens. Bioelectron.* **2014**, *59*, 40.
[36] S. Krishnamurthy, A. Esterle, N. C. Sharma, S.V. Sahi, *Nanoscale Res. Lett.* **2014**, *9* (1), 1.
[37] G. Liu, T. Gredig, I. K. Schuller, *EPL* **2008**, *83* (5), 56001.
[38] X. F. Zhang, Y. Di, F. Zhang, *J. Photochem. Photobiol. A* **2009**, *203* (2-3), 216.
[39] X. F. Zhang, X. Li, L. Niu, L. Sun, L. Liu, *J. Fluoresc.* **2009**, *19* (6), 947.
[40] T. P. Mthethwa, S. Tuncel, M. Durmuş, T. Nyokong, *Dalton Trans.* **2013**, *42* (14), 4922.
[41] W. Spiller, H. Kliesch, D. Wöhrle, S. Hackbarth, B. Röder, G. Schnurpfeil, *J. Porphyr. Phthalocyanines* **1998**, *02* (02), 145.
[42] Ö. Tayfuroğlu, F. A. Kılıçarslan, G. Y. Atmaca, A. Erdoğmuş, *J. Porphyr. Phthalocyanines* **2018**, *22* (01n03), 250.
[43] E. Dube, D. O. Oluwole, E. Prinsloo, T. Nyokong, *New J. Chem.* **2018**, *42* (12), 10214.
[44] E. Dube, T. Nyokong, *J. Lumin.* **2019**, *205*, 532.
[45] G. Pasparakis, *Small* **2013**, *9* (24), 4130.
[46] R. Vankayala, A. Sagadevan, P. Vijayaraghavan, C. L. Kuo, K. C. Hwang, *Angew. Chem. Int. Ed.* **2011**, *50* (45), 10640.

Manuscript received: November 16, 2023
Revised manuscript received: December 22, 2023
Version of record online: ■■, ■■

RESEARCH ARTICLE

Zinc phthalocyanine is covalently linked to plasmonic AuNPs via click chemistry to investigate the synergistic effect that boosts the overall activity toward the detection of HQ under visible light illumination. The $^1O_2$ quantum yield of ZnPc improved significantly after conjugating with AuNPs, resulting in enhanced photoelectrochemical activity.

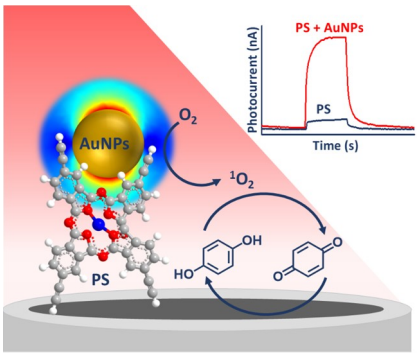

*S. U. Khan, R. Matshitse, R. Borah, M. Nemakal, E. O. Moiseeva, T. V. Dubinina, T. Nyokong, S. W. Verbruggen, K. De Wael**